Research Square

Preprints are preliminary reports that have not undergone peer review.
They should not be considered conclusive, used to inform clinical practice,
or referenced by the media as validated information.

Three-dimensional Model Fitting to Magnetic Clouds for Multiple In Situ Spacecraft Measurements

Qiang Hu

qh0001@uah.edu

University of Alabama in Huntsville

Research Article

Keywords: Coronal Mass Ejections, Interplanetary, Magnetic fields, Interplanetary, Magnetic fields, Models, Plasma Physics

Posted Date: November 6th, 2026

DOI: https://doi.org/10.21203/rs.3.rs-11354363/v1

License: This work is licensed under a Creative Commons Attribution 4.0 International License.
Read Full License

Additional Declarations: No competing interests reported.

Three-dimensional Model Fitting to Magnetic Clouds for Multiple In Situ Spacecraft Measurements

Qiang Hu[1]

© **The author(s)** ●●●●

Abstract We have performed an optimal model fitting analysis to a magnetic cloud (MC) event on December 1-3, 2023, when Wind and STA spacecraft crossed the same structure along closely separated paths. The Solar Orbiter (Sol) spacecraft, with a relatively larger separation distance from Earth (Wind), also appeared to have crossed the same structure at an earlier time. The analytic model employed for the optimal fitting to the magnetic field data is based on a linear force-free field formulation, possessing three-dimensional (3D) spatial variations, and is dubbed Friedberg solution (FS). By employing both Wind and STA in-situ measurements along their separate paths across the same MC structure, we obtain the set of parameters characterizing the FS model fit with an optimal reduced χ^2 value of 3.60. We then compare the FS model output along the STA spacecraft path with the actual magnetic field measurements and obtain a correlation coefficient, cc_1 =0.94 - 0.96. By examining the magnetic field line configuration more closely, we also find that the Sol spacecraft may have crossed the same MC body along its path at a relatively larger distance away from the Wind spacecraft path and over a shorter time interval. A similar comparison between the FS model output and the Sol data yields a correlation coefficient cc_2 =0.81 - 0.90. For completeness, we also perform the two-dimensional (2D) Grad-Shafranov (GS) reconstruction of the MC structure by using the Wind spacecraft data only. A similar analysis yields cc_1 =0.93 - 0.96, and $cc_2 = -0.37$ - 0.11 for the GS reconstruction result. Hence our interpretation is that the analysis results based on three spacecraft datasets are consistent with the 3D spatial magnetic field configuration of the FS model output for this MC event to the degree indicated by the aforementioned quantitative metrics.

Keywords: Coronal Mass Ejections, Interplanetary; Magnetic fields, Interplanetary; Magnetic fields, Models; Plasma Physics

---

✉ Qiang Hu
qh0001@uah.edu

[1] Department of Space Science, The University of Alabama in Huntsville, Huntsville, AL 35805, USA

1. Introduction

Magnetic clouds (MCs) are a type of interplanetary coronal mass ejections (ICMEs) possessing a distinctive set of observational signatures based on in-situ spacecraft measurements (Burlaga 1988; Lepping, Burlaga, and Jones 1990; Burlaga 1995; Lepping et al. 1997). They are large-scale structures corresponding to CME eruptions from the Sun. They have been routinely identified and classified from the in-situ spacecraft measurements since the early years of the space age and have been studied for decades with the increasing amount of data returned from the past and on-going heliospheric spacecraft missions. These include the NASA flagship Advanced Composition Explorer (ACE), Wind, Solar TErrestrial RElations Observatory (STEREO with two probes, STA and STB, in short), Parker Solar Probe (PSP), and the latest joint NASA/ESA mission, Solar Orbiter (Sol). They cover a wide range of heliocentric distances and heliographic longitudes in the inner heliosphere, which enables enhanced capability in detecting ICMEs/MCs. Some recent effort has resulted in well-organized categorization of ICME events from multiple spacecraft missions that is of great utility, e.g., the Helio4cast ICME catalogue (Möstl et al. 2026). There is a great deal of variability in the in-situ measurements of MC structures, when they pass an observing spacecraft, as manifested in both the magnetic field and particle/plasma time-series data. Therefore this necessitates the need for the MC models based on in-situ spacecraft measurements to possess adequate level of complexity to account for the intrinsically two-dimensional (2D) or three-dimensional (3D) magnetic field configurations.

A fully 2D model for MCs based on the Grad-Shafranov (GS) equation has been applied to derive a 2D cross section of a cylindrical configuration since the early 2000s (Hu and Sonnerup 2001, 2002). It is similar to a model fitting method in that it also employs the in-situ data along a spacecraft path across an MC interval, but differs in that it solves for a numerical solution of magnetic field governed by the GS equation without explicitly specifying an analytic form of the solution. Such a solution is fully characterized by a 2D scalar flux function A, due to the translation symmetry in the axial dimension for a cylindrical geometry, analogous to an incompressible flow field for which the transverse flow is represented by a scalar stream function. The development and a complete documentation of the GS method as applied to MCs were presented in Hu and Sonnerup (2002) based on the initial development by Hau and Sonnerup (1999) and Sonnerup and Guo (1996). A comprehensive review of the GS-based methodology for in-situ spacecraft data analysis and its applications, not limited to MC modeling, was provided by Hu (2017).

One recent attempt to increase the complexity of the MC models to account for 3D spatial variations was made by adopting an analytic formulation for the MC magnetic field with 3D spatial dependence. The formulation is based on an expanded solution to a linear force-free field in cylindrical coordinates and provides an explicit solution for the magnetic field with 3D spatial dependence and a set of free parameters (Freidberg 2014). Thus a standard least-squares minimization approach is commonly taken to obtain the optimal set of parameters which determines the solution that best fits the spacecraft measurements (all three

components of the magnetic field) along its path across the MC structure. Such an approach employing the 3D analytic solution, dubbed "Freidberg Solution" (FS) (Freidberg 2014), was first developed in Hu et al. (2021); Hu (2021). It was applied in a comprehensive analysis of a flare/CME and ICME/MC connection event in Hu et al. (2022) by employing multiple spacecraft datasets including both remote-sensing and in-situ observations. It revealed the 3D characteristics of the magnetic flux rope configuration for MC, i.e., that of a "twisted ribbon" beyond a 2D cylindrical topology. A few follow-up studies demonstrated the feasibility of this approach and its application in relating to solar source properties (Hu et al. 2021; He et al. 2022; Hu 2023). In particular, an approach of employing two-spacecraft datasets of simultaneous magnetic field measurements along two distinct paths across one MC structure was applied successfully for another event study (Hu, He, and Chen 2022).

To further demonstrate the necessity of adequate complexity in MC models based on in-situ data, and the coordinated use of multiple (≥ 2) spacecraft measurements simultaneously, we present an additional event study here, specifically with three spacecraft datasets involved for one MC event. We aim to address and/or raise awareness of the following main points: 1) whenever possible, it is necessary to apply and combine simultaneous in-situ measurements from more than one spacecraft for MC modeling and model validation, and 2) it remains a challenging question whether such a validation is sufficient to yield a unique solution for the magnetic field topology of the MC. This article is organized as follows. We present an overview of the MC event and the analysis methods to be applied in Section 2. The result from the simultaneous fitting by the FS model to two-spacecraft datasets (from both Wind and STA) is presented in Section 3. For completeness, we show the 2D GS reconstruction result in Section 4. We conclude our interpretation for this event study in the last section.

2. Event Overview and Methodology

The selected MC event occurred during December 1 to 3, 2023, reaching 1 AU when three spacecraft located near Earth, namely, Wind, STA and Sol. Figure 1 shows the locations of multiple spacecraft on the ecliptic plane at that time, including those three around Earth (see Solar-MACH web portal[1] for detailed information about their specific location coordinates). Around that time, STA was separated from Earth by $\sim 6.4°$ in longitude to the West at a heliocentric distance of 0.97 AU. Sol was about 10° to the East at a heliocentric distance of about 0.85 AU.

Figure 2 shows the corresponding time-series measurements from Wind spacecraft during a time period of several days. They include the typical set of interplanetary magnetic field and bulk solar wind plasma parameters at 1 AU, together with the additional measurement of the suprathermal electron pitch angle distributions (ePADs) for electrons of energy ∼255 eV. The vertical lines

[1] https://da.gd/CPzMJ

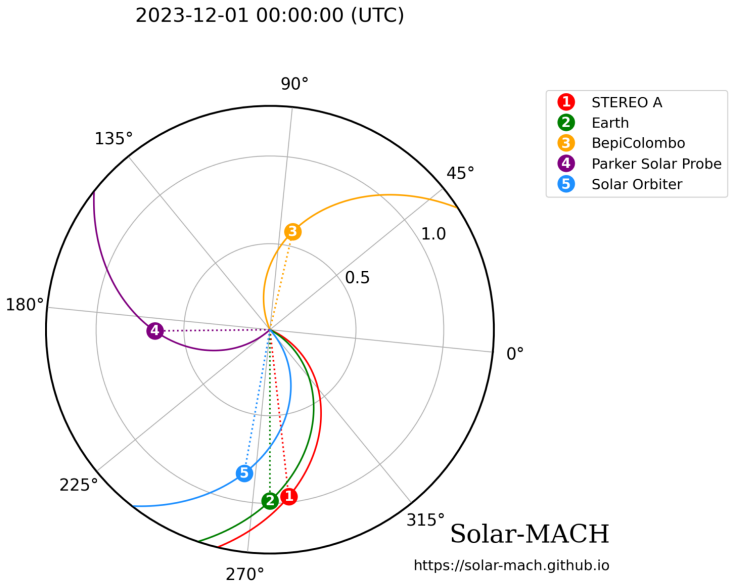


Figure 1. The multiple spacecraft locations (see the legend) on December 1, 2023 on the ecliptic plane, as generated by Solar-MACH (Gieseler et al. 2023). The spacecraft STA, Wind ("Earth") and Sol located closely around Earth at that time.

mark the analysis interval chosen for obtaining the final results to be presented. It represents an interval possessing the typical observational signatures for an MC: 1) enhanced magnetic field magnitude, 2) a relatively smooth rotation in the field direction, and 3) depressed proton temperature and proton β. The ePADs show relatively intensified streaming electrons in the anti-field direction (near 180°), indicative of field-line connectivity back to the Sun at one end during the passage of the MC structure.

This interval was chosen following a process of repeated analysis of multiple intervals that are valid choices (see, e.g., Hu et al. 2022). The process starts by setting the boundaries for the ranges of the beginning and ending times of the possible analysis intervals. Then each interval is taken in turn by pairing up the times, separated by, e.g., 1 hour, in each range, for this event. It resulted in a total number of 63 different intervals for the repeated analysis. The analysis was performed by using the single Wind spacecraft dataset alone for an FS model fitting approach to be described below. The outputs for all different intervals are too cumbersome to be presented here, but can be provided upon request. After assessing the quality of the fitting results and taking into account the additional (both STA and Sol) spacecraft paths across presumably the same MC structure, one interval is chosen as given in Figure 2 and the final analysis results for this interval are reported in the following sections. Figure 3 shows the similar set of in-situ measurements from STA, with the corresponding MC interval marked, determined after considering proper time shift between Wind and STA spacecraft. The STA time-series data show very similar features for the MC interval, owing to the close proximity between the two probes.

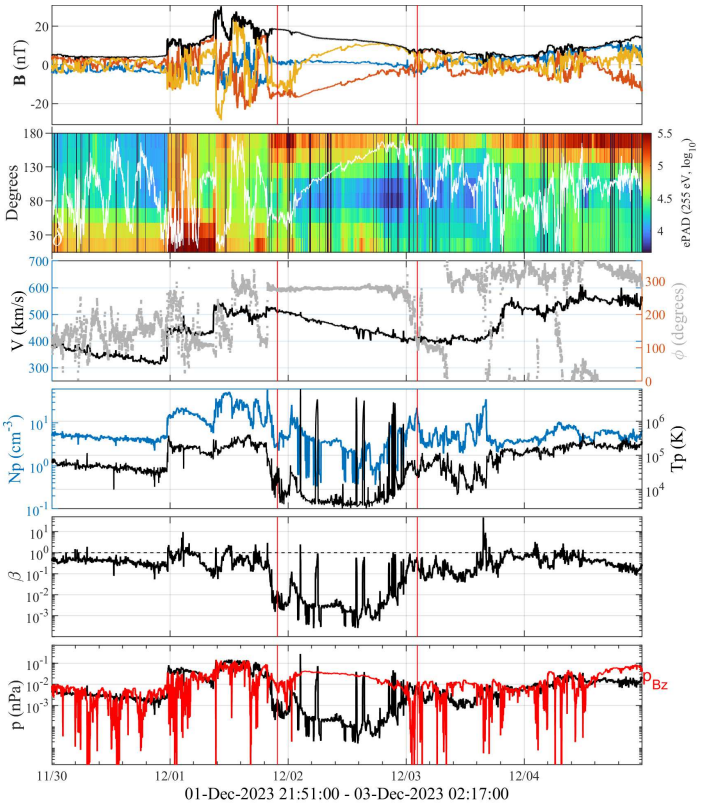


Figure 2. Time-series data from Wind spacecraft between November 30 and December 5, 2023. From top to bottom, the panels are the magnetic field magnitude (in black) and the components in the Geocentric Solar Ecliptic (GSE) coordinates (X, in blue, Y, in red, and Z, in gold), the electron pitch angle (in degrees) distribution (ePAD) with the polar angle of the magnetic field direction overlaid by the white curve, the solar wind speed (black curve, left axis) and the azimuthal angle of the magnetic field direction (gray curve, right axis), the proton density (left axis) and temperature (right axis), the proton β, and the proton/axial magnetic pressure in black/red. The vertical red lines mark the MC event analysis interval in UT as denoted beneath the bottom panel.

The FS model fitting approach is to employ a standard χ^2 least-squares minimization algorithm to derive the set of free parameters for an analytic solution of the magnetic field given below, by minimizing the difference between the analytic and measured magnetic field components along one or multiple spacecraft paths across one MC structure. The method has been developed and applied in a number of prior studies (see Hu 2021, for detailed description of the procedures). For completeness, we repeat the FS formulation below in a cylindrical coordinate system (r, θ, z) (Freidberg 2014):

$$\frac{B_z(\boldsymbol{r})}{B_{z0}} = J_0(\alpha r) + CJ_1(lr)\cos(\theta + kz), \tag{1}$$

$$\frac{B_\theta(\boldsymbol{r})}{B_{z0}} = J_1(\alpha r) - \frac{C}{l}\left[\alpha J_1'(lr) + \frac{k}{lr}J_1(lr)\right]\cos(\theta + kz), \tag{2}$$

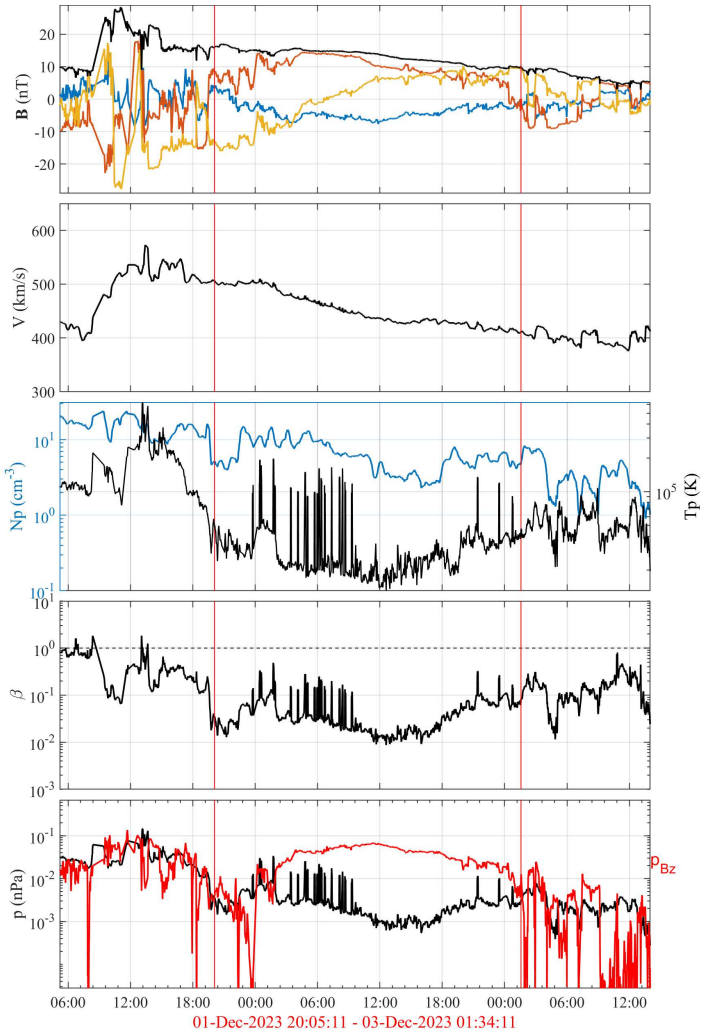


Figure 3. Time-series data from the STA spacecraft between ∼06:00 UT, December 1 and ∼12:00 UT, December 3, 2023. The panels are, similarly to Figure 2 from the top to bottom, the magnetic field magnitude and components in the local Radial (in blue), Tangential (in red), and Normal (in gold; RTN) coordinates, the solar wind speed, the proton density and temperature, the proton β, and the proton/axial magnetic pressure. The analysis interval as marked by the vertical red lines is denoted beneath the bottom panel.

$$\frac{B_r(\boldsymbol{r})}{B_{z0}} = -\frac{C}{l}\left[kJ_1'(lr) + \frac{\alpha}{lr}J_1(lr)\right]\sin(\theta + kz). \tag{3}$$

Here the constant parameters are a proportionality factor C for the field components after a normalization by B_{z0}, the linear force-free constant α, a wavenumber in the z dimension, k, and $l = \sqrt{\alpha^2 - k^2}$. The latter three are normalized by a length scale, a, characteristic of the approximate cross-section size of the structure (Hu 2021). Such a solution possesses dependence on all three spatial

dimensions, albeit it is periodic in the z dimension. Therefore strictly speaking, the spatial configuration is regarded as "quasi-3D", but we use the term "3D" inter-changeably in this presentation.

For one spacecraft dataset, the standard χ^2 function is given by (Press et al. 2007),

$$\chi^2 = \frac{1}{\texttt{dof}} \sum_{\nu=X,Y,Z} \sum_{i=1}^{N} \frac{(b_{\nu i} - B_{\nu i})^2}{\sigma_i^2}, \tag{4}$$

where the discrete time-series magnetic field data are represented by $\boldsymbol{b}_i$, with an integral index i for the data arrays of length N. The data points for analysis are usually of a resolution around an hour and are averaged from higher-resolution (e.g., 1-miniute) magnetic field data $\tilde{\boldsymbol{b}}$ over each hourly interval, i.e. $\boldsymbol{b}_i = \langle \tilde{\boldsymbol{b}} \rangle_{(i\text{th hour})}$ $(i \in [1, N])$. The degree of freedom, $\texttt{dof}$, is of the value $3N-n-1$, where the number of free parameters is denoted n (Hu 2021). The associated uncertainties σ_i are estimated through the same process for each hourly interval by the corresponding root-mean-square (RMS) values of the higher-resolution magnetic field components, i.e. $\sigma_i^2 = \sum_\nu \langle (\tilde{b}_\nu - \langle \tilde{b}_\nu \rangle)^2 \rangle_i$. It is worth noting that the uncertainties for this analysis are not absolute errors from the instrumentation, which is generally much less than 1 nT for magnetometers. The RMS values described here represents an estimation of the level of fluctuations superposed on the large-scale MC structure which has more gradual or smoother variations and is what we are aiming to model.

This minimization procedure is readily applicable to multiple (≥ 2) spacecraft datasets simultaneously by constructing the χ^2 function through simple addition of individual χ^2 function given by equation (4) for each spacecraft along its separate path across the same structure,

$$\chi^2 = \chi_1^2 + \chi_2^2 + ... \tag{5}$$

The same optimization algorithm applies and yields one set of model parameters at once to best fit the multiple in-situ spacecraft datasets in the least-squares sense.

3. Two-Spacecraft FS Model Fitting Result

In this section, we present the results obtained by performing a two-spacecraft optimization by employing the FS model and the magnetic field measurements from both Wind and STA, as described in the previous section. We also present a correlation analysis for the magnetic field between the FS model output and the actual spacecraft data along the STA and Sol paths. Table 1 summarizes the set of parameters obtained for the optimal FS model fitting result based on equations (1) to (5) by employing both Wind and STA magnetic field measurements along their separate paths. The constant value for B_{z0} is 16 nT. The corresponding 90% confidence limits are also assessed following Press et al. (2007).

Table 1. Selected parameters from the two-spacecraft FS model fitting result.

Parameters[1]	C	$\hat{\mathbf{z}}^2$	k	α
	-85	(70, 328)°	-1.945909	1.945914
90% Conf. Limit	±1.7	±(9,10)°	±0.0002	±0.0002

[1]The parameters C, k, and α as listed are dimensionless with the latter two normalized by a length scale, $a = 0.15$ AU.
[2]The z axis orientation given by the pair of polar angle measured from the ecliptic north, and the azimuthal angle measured from GSE-X towards GSE-Y axes, all in degrees.

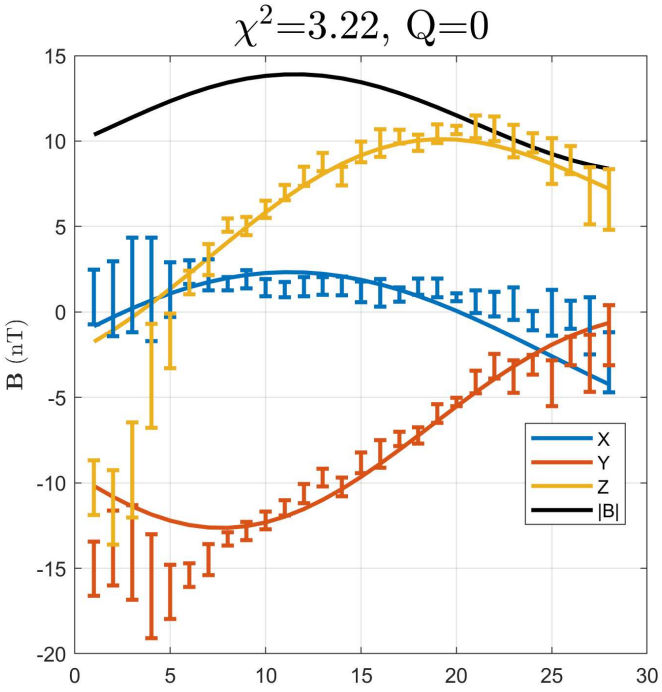


Figure 4. The two-spacecraft optimal fitting result of the magnetic field components along the Wind spacecraft path as denoted by the legend. The FS model result is represented by the smooth curves, while the spacecraft measurements with uncertainties are marked by discrete points with errorbars. The x axis shows the array indices.

Figure 4 shows the standard optimal χ^2 fitting result obtained by employing both Wind and STA magnetic field measurements for their respective MC intervals, based on equation (5), but for the Wind magnetic field measurements downsampled to 1 hour resolution in the GSE coordinates. The corresponding minimum reduced χ^2 value for this data segment and the associated quality factor, Q, value are given on top. Strictly speaking, the result carries significant statistical uncertainty because of the small Q value ($<< 1$) due to model limita-

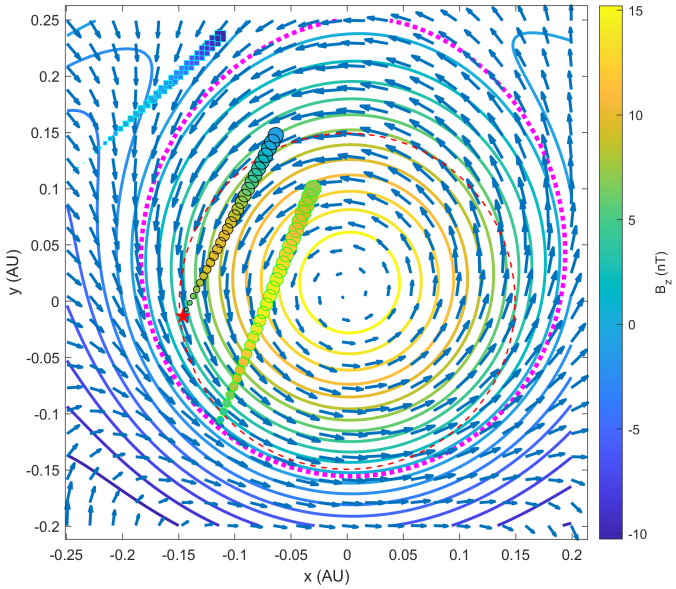


Figure 5. One cross section (at $z = 0$) of the FS model result for the magnetic field as viewed down the z axis. The arrows show the transverse field and the colored contours show the axial field distribution on this plane as indicated by the colorbar. The magenta dotted curve indicates the contour where B_z=0. The three sets of symbols mark the separate spacecraft paths for Sol, Wind, and STA, from left to right, respectively. Along each path, the symbols are color coded by the local B_z components according to the colorbar, and the size for each symbol is approximately proportional to its relative distance from the viewer (the smaller the farther away). The starting location for Wind is marked by the red star.

tions, according to Press et al. (2007). In practice we proceed with the validation process by further comparing the analytic model output with additional spacecraft datasets, considering the fact that it is not guaranteed that the magnitude of the χ^2 value is an absolute indicator of the "goodness" of a solution.

Figure 5 shows one cross section at $z = 0$ within certain (x, y) domain. Different from a 2D solution, such a cross section configuration for the FS model varies with the z dimension. In addition, the three spacecraft paths as shown in this projected view are not lying in one plane perpendicular to the z axis. Both Wind and STA spacecraft may have crossed near the "center" of the structure where the axial field strength reaches the maximum, while Sol's path is farther away. Note that in this quasi-3D configuration, still possessing general similarity to a flux rope structure with spiral field lines as indicated by the transverse and axial field components, the center of the structure is no longer a straight field line. These points are further illustrated by the 3D visualization of field-line configuration in Figure 6, where several sets of individual field lines are

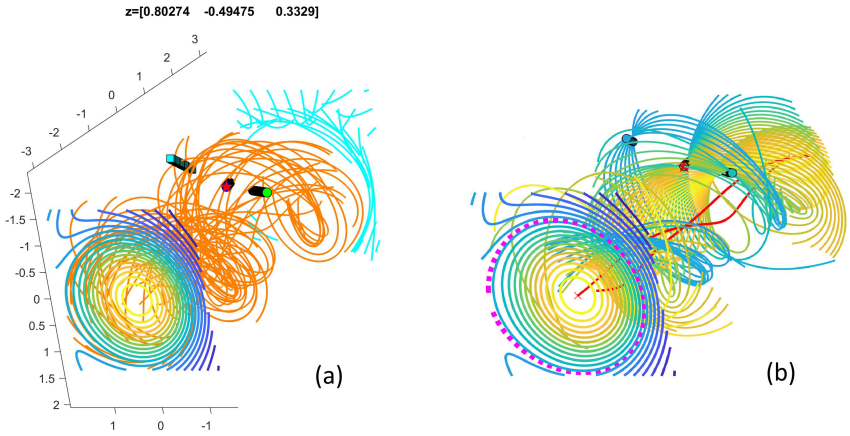


Figure 6. 3D field-line plot for the FS model result along a viewpoint toward Sun from Earth (East-West direction is horizontal). (a) The orange lines show field lines originating from the main positive polarity region with $B_z > 0$ on the bottom plane where the contours of B_z are drawn, while the cyan lines show field lines originating from the surrounding negative polarity region near the top. The cylindrical axis orientation is given on top in the GSE coordinates. (b) The same view as (a) but with only selected field lines threading the three spacecraft paths shown and they are color-coded by the local B_z component along each path as indicated in Figure 5. Two field lines rooted near the center of the bottom plane where B_z is the maximum are also drawn in red. The same sets of symbols for the three spacecraft paths as Figure 5 are also shown in this view.

drawn including the ones in red originating near the center, and viewed from the perspective of Earth toward Sun. In this view, the MC structure exhibits one main flux bundle of spiral field lines with one polarity winding in the direction toward the Sun. The three spacecraft appear to have sampled the flux bundle at different spatial locations. Threaded along their separate paths, the field lines are winding and forming twisted-ribbon like structures. In particular as seen in Figure 6, right panel, the red field lines originating at and near the point where the axial field reaches the maximum on the bottom cross section plane are winding along the z dimension as well. This is a characteristic feature distinctive from a 2D configuration where the spatial variation in the z dimension is not present.

With the full model solution known as presented in Table 1, Figures 5 and 6, it is desirable to compare the FS model output along the STA and Sol spacecraft paths with their respective measurements. Figure 7 shows such a comparison for the STA magnetic field data with the corresponding range of correlation coefficient denoted, cc_1 = 0.94-0.96. The range is obtained by a simple and effective bootstrap uncertainty estimate approach (Kawano and Higuchi 1995). For Sol, it took us some additional effort to identify the interval for such a correlative analysis from the time-series data. In Figure 8, we show the time-series measurements from Sol for a 3-day time period. By visual inspection, a similar comparison for an extended time period of a day or so for the MC structure at Sol is questionable (see also Figure 9). Based on the signatures in the proton temperate T_p and the B_{rms} values, a shorter interval with both

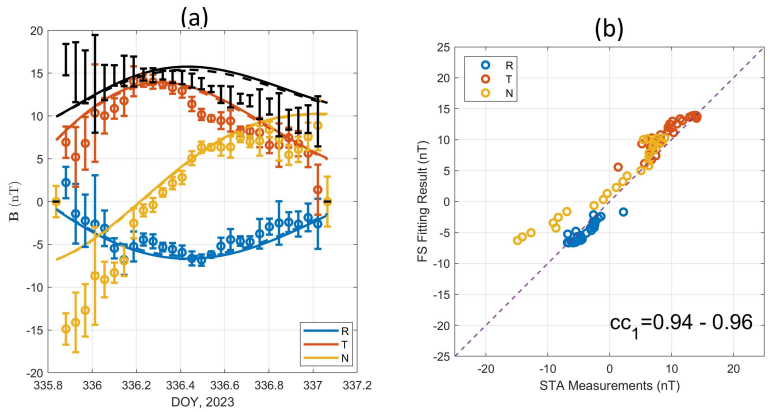


Figure 7. (a) The corresponding FS model fitting result for STA along its path. The format is the same as Figure 4, but with the x axis given in day of year (DOY). (b) The component-wise comparison of magnetic field between the FS model result and the STA measurements. The dashed diagonal line indicates perfect agreement. The corresponding correlation coefficient is denoted by cc_1.

depressed T_p and B_{rms} (representative of magnetic field fluctuations) seems to be more likely corresponding to the MC structure. Therefore, in Figure 9, right panel, we show the same correlative analysis result for this shorter interval as marked in the left panel, and obtain the corresponding correlation coefficient, cc_2 =0.81-0.90, for the Sol magnetic field data.

To further demonstrate that indeed this shorter interval corresponds to the crossing of the main MC structure by Sol as depicted by the main flux bundle in Figure 6, we take a closer look and present in Figure 10 with three different view angles, the field lines threading the Sol path only. Indeed the field lines passing the Sol path during that short interval all spiral down and end on the cross-section plane within the boundary of the main flux bundle. Therefore we conclude that the Sol did cross the same main MC structure as encountered by the other two spacecraft, albeit over a short interval of about 7 hours at a larger separation distance from Earth in this event.

4. GS Reconstruction Result

For completeness and also for additional comparisons with a 2D model output, we perform the GS reconstruction of the MC structure using the Wind spacecraft measurements for the same interval marked in Figure 2. We refer interested readers to Hu (2017) for the technical details and to the documentations for a software package, PyGS[2], implemented in Python. Figures 11 and 12 show the standard output of the GS reconstruction results for this MC event. In Figure 11, a single-variable functional relation between $P_t = p + B_z^2/2\mu_0$, the

[2]Available through GitHub and PyHC, https://heliopython.org/

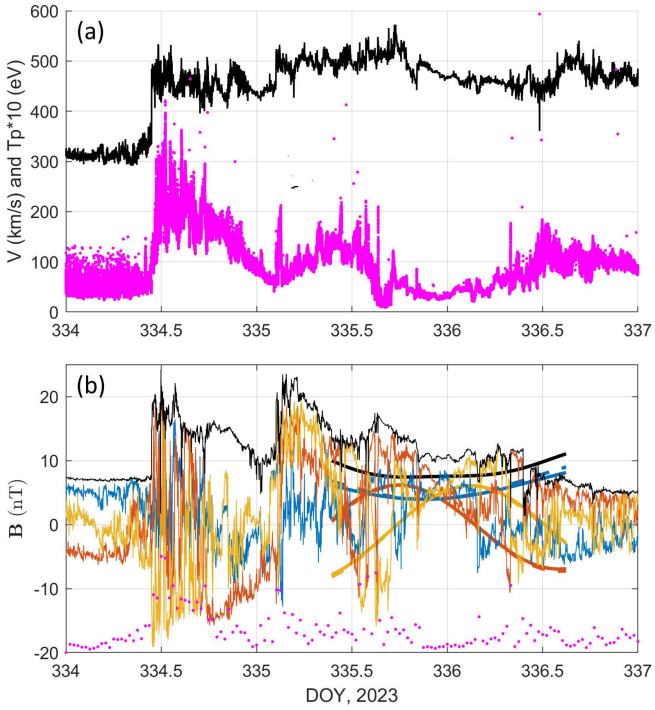


Figure 8. Time-series data for Sol during November 30 (DOY 334) and December 3 (DOY 337), 2023. (a) The solar wind speed (black curve) and the proton temperature (×10 eV; magenta curve). (b) The magnetic field components and magnitude (in black) in the spacecraft centered RTN coordinates (R, in blue, T, in red, and N, in gold). The magenta dots near the bottom show the relative magnitudes of the RMS values of the magnetic field. The thick smooth curves show the corresponding FS model result for an extended interval along the Sol spacecraft path.

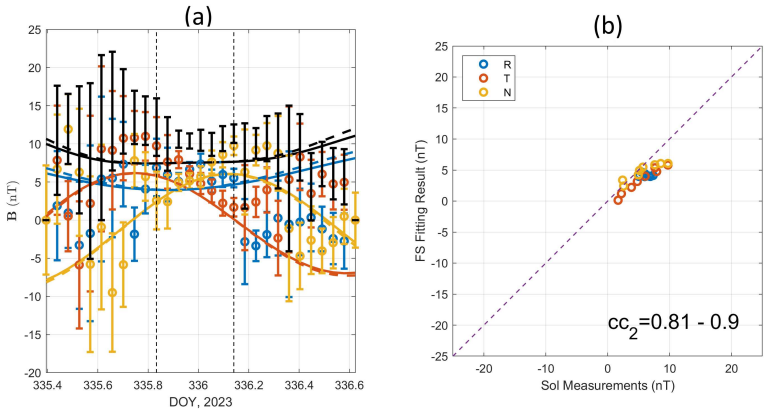


Figure 9. (a) Format is the same as Figure 7a for Sol for the extended interval. A shorter interval between DOYs 335.833 and 336.140 is marked by the vertical dashed lines and the corresponding correlation plot for this shorter interval is given in (b) with the correlation coefficient cc_2 denoted.

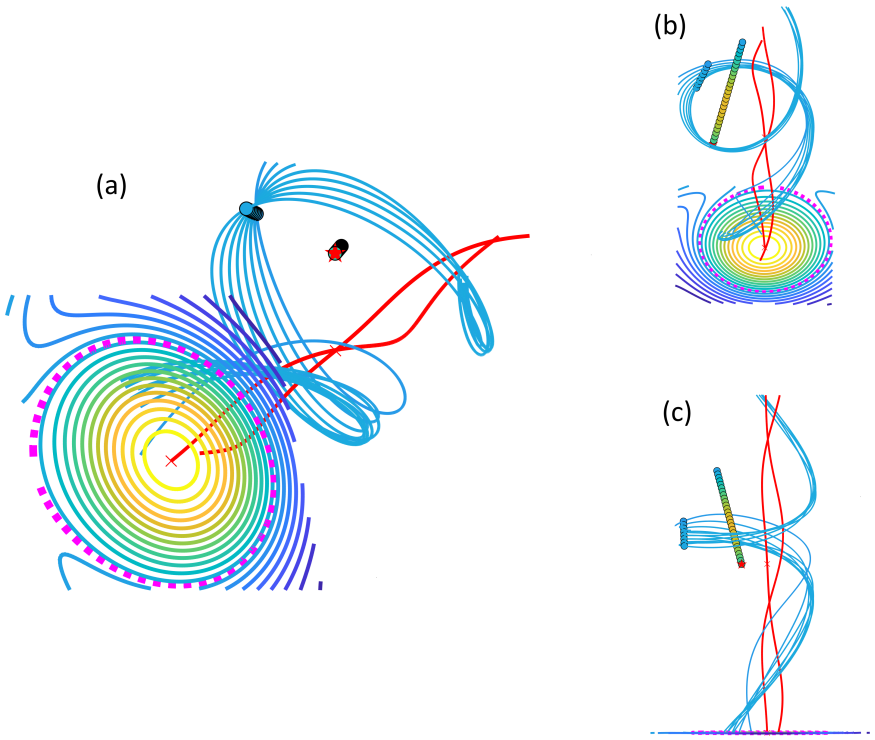


Figure 10. (a) The same plot as Figure 6b, but with only the selected field lines threading the shorter interval along the Sol path shown. Panels (b) and (c) are the same plots, but for different view angles. The symbols are lining along the Sol and Wind spacecraft paths, respectively.

sum of plasma pressure and the axial magnetic pressure, and the flux function A, along the spacecraft path, is obtained for an optimally determined z axis orientation ($\hat{\mathbf{z}}$ =[0.3867, -0.8354, 0.3905] in the GSE coordinates). A fitting residue $R_f = 0.10 << 1.0$ for $P_t(A)$ is denoted and considered acceptable (Hu 2017), which serves as a sufficient condition for the GS reconstruction result to be a valid 2D solution. Figure 12 shows the corresponding solution on the cross section plane where all three components of the magnetic field are shown in the local coordinates (x, y, z) within a 2D domain with no spatial variation in z (i.e., $\partial/\partial z = 0$). It represents a view down the z axis of a cylindrical magnetic field configuration with nested distinct flux surfaces characterized by the flux function A, on which magnetic field lines are winding around a central axis along z. The field line originating from the red dot is a straight line, corresponding to the central axis (or the "center"). This configuration is typical of a (2D) flux rope topology where the distinct flux surfaces are readily identified and well organized with translation symmetry. The projected STA and Sol spacecraft paths indicate that the STA path is close to the center of the flux rope while the Sol path is father away and outside the boundary (where $A = A_b$) of such a 2D flux rope

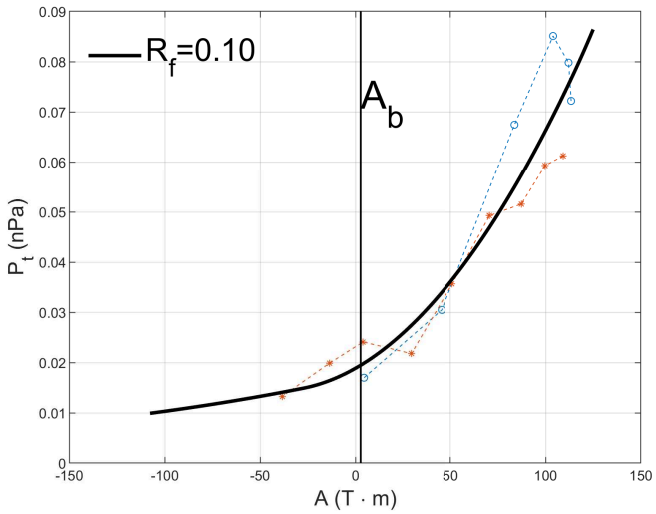


Figure 11. The plot of transverse pressure P_t versus the flux function A along the Wind spacecraft path for the GS reconstruction result. The symbols represent the measured data points while the black curve shows a functional fitting of $P_t(A)$ with the corresponding fitting residue R_f denoted. The vertical line marks the value $A = A_b$ for a flux surface chosen as the boundary of a valid GS solution.

structure. This boundary value, marked in Figure 11, represents a specific flux surface beyond which the 2D geometry is no longer considered valid for $A < A_b$ in this case because of the possible violation of the requirement that $P_t(A)$ be approximately single-valued as judged by Figure 11.

The corresponding correlative analyses similar to those done in Section 3 are carried out for the STA and Sol magnetic field measurements over the same intervals. Figures 13 and 14 present these analysis results for STA and Sol, respectively, in the same format as before. The correlation coefficient $cc_1 = 0.93$ - 0.96 is comparable with the value obtained for the FS model. The correlation coefficient $cc_2 = -0.37$ - 0.11, however, is much inferior to the one resulted from the FS model comparison.

5. Summary and Interpretation

In summary, we have analyzed an MC event by applying the quasi-3D FS model for the magnetic field configuration to the in-situ measurements from three spacecraft, the Wind, STA and Sol. The STA and Sol spacecraft were separated from Wind by about ~ 6.4 and ~ 10 degrees to the West and East in longitudes, respectively. We obtain an optimal fitting result by employing both Wind and STA magnetic field measurements along their separate paths through a formal χ^2 minimization approach. The solution yields a magnetic field configuration exhibiting spiral field lines with 3D spatial variations. It comprises a main flux bundle with a single polarity, possessing an overall winding along the z dimension

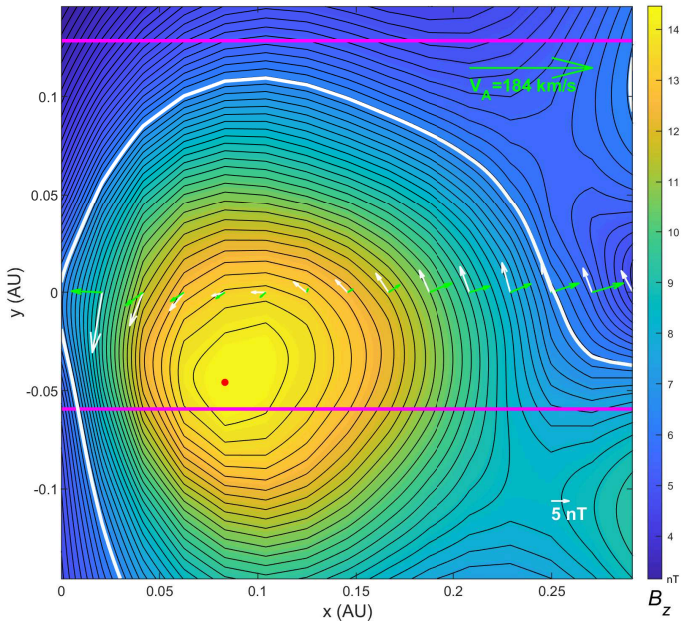


Figure 12. The cross section map of the GS solution for the magnetic field distribution. The black contour lines are the contours of $A(x, y)$, i.e., the transverse field lines on the (x, y) plane. The filled color contours are the distribution of B_z with scales indicated by the colorbar. The white (green) arrows along $y = 0$ (the projected spacecraft path) represent the measured transverse magnetic field (velocity) with reference vectors, a constant field of 5 nT and the average Alfvén velocity, respectively, denoted near the bottom right (top right). The top and bottom magenta lines are the projected Sol and STA spacecraft paths, respectively. The thick white contour marks the boundary where $A = A_b$ and the red dot indicates the center where the axial field B_z reaches the maximum.

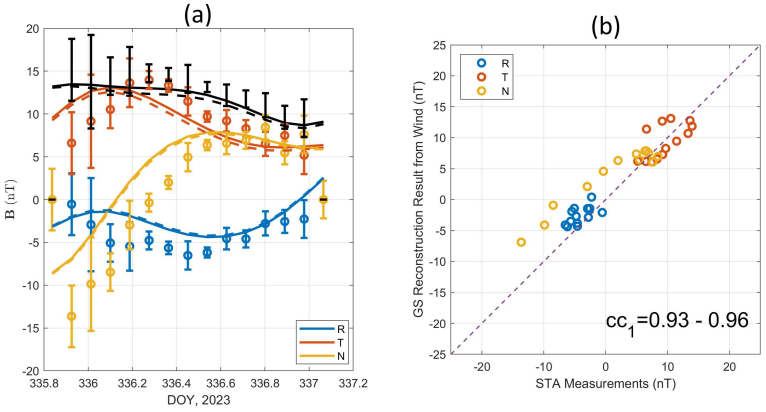


Figure 13. The comparison between the measured magnetic field and the GS reconstruction result along the STA spacecraft path. Format is the same as Figure 7.

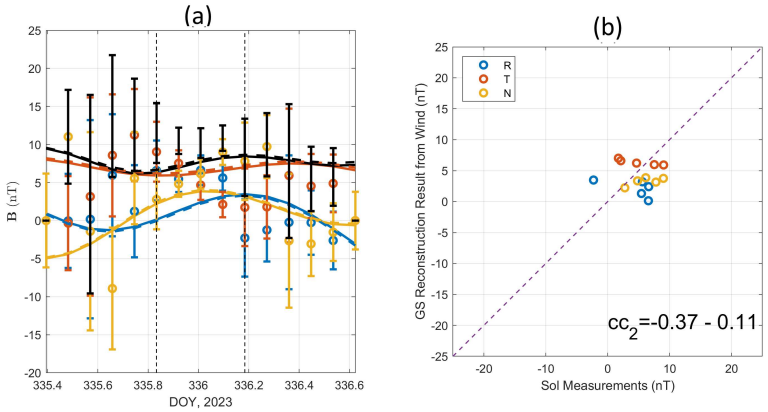


Figure 14. The comparison for Sol magnetic field data along its path with the GS reconstruction result. Format is the same as Figure 9.

for all field lines. In particular, there lacks a straight field line corresponding to the center of a flux rope structure, typical of a 2D configuration with translation symmetry in the axial dimension, as represented by the corresponding GS reconstruction result from Wind. In addition, their z-axis orientations differ by about 30 degrees. In the accompanying correlative analyses against the STA dataset for the two model results, both yield a correlation coefficient $cc_1 > 0.9$ between the model output and the measured magnetic field components along its path. Whereas for the similar comparison with the Sol dataset, the corresponding correlation coefficient cc_2 is about 0.9 for the FS model output, while it deteriorates to $\lesssim 0.1$ for the GS reconstruction result.

Based on these quantitative analysis results, and detailed topological analysis and visualization (see Figures 6 and 10), we therefore interpret this MC event as an occurrence near 1 AU intercepted by three spacecraft with small to modest separation distances from one another. The spatial variations seen in the in-situ time-series measurements from the three spacecraft are attributed to the 3D magnetic field configuration of the main MC structure. The FS model output with the set of optimal parameters is found to be consistent with three in-situ spacecraft datasets over their respective time intervals and thus represents such an MC structure in this event to the degree quantified by the relevant metrics. However whether this is sufficient to prove that the magnetic field topology obtained by the FS model fitting to the Wind-STA datasets represents the ground truth is still not absolutely certain, although such a multi-spacecraft data analysis lends confidence in the solution over limited local scales near the vicinity of the spacecraft passages. Yet the solution presented illustrates the complexity necessary for MC models in order to account for the 3D spatial variations commonly manifested in the in-situ spacecraft measurements across MC structures. This analysis also further advocates the utilization of multiple spacecraft datasets whenever possible.

Acknowledgements QH acknowledges partial support of NASA grants 80NSSC21K1763, and 80NSSC21K0003. The authors also thank Dr. Hiroshi Hasegawa for directing us to the bootstrap method of Kawano and Higuchi (1995).

Author Contribution QH initiated and carried out this study, and completed the manuscript by his solo effort.

Funding NASA grants 80NSSC21K1763, and 80NSSC21K0003.

Data Availability All the in-situ spacecraft measurements employed are available online through the NASA CDAWeb data depository.

References

Burlaga, L.F.: 1988, Magnetic clouds and force-free fields with constant alpha. *Journal of Geophysical Research: Space Physics* **93**, 7217. DOI. https://agupubs.onlinelibrary.wiley.com/doi/abs/10.1029/JA093iA07p07217.

Burlaga, L.F.: 1995, Interplanetary magnetohydrodynamics. *Interplanetary magnetohydrodynamics, by L. F. Burlag. International Series in Astronomy and Astrophysics, Vol. 3, Oxford University Press. 1995. 272 pages; ISBN13: 978-0-19-508472-6* **3**. ADS.

Freidberg, J.P.: 2014, *Ideal MHD*, Cambridge University Press, Cambridge, UK, 546.

Gieseler, J., Dresing, N., Palmroos, C., Freiherr von Forstner, J.L., Price, D.J., Vainio, R., Kouloumvakos, A., Rodríguez-García, L., Trotta, D., Génot, V., Masson, A., Roth, M., Veronig, A.: 2023, Solar-MACH: An open-source tool to analyze solar magnetic connection configurations. *Frontiers in Astronomy and Space Sciences* **Volume 9 - 2022**. DOI. https://www.frontiersin.org/journals/astronomy-and-space-sciences/articles/10.3389/fspas.2022.1058810.

Hau, L.-N., Sonnerup, B.U.Ö.: 1999, Two-dimensional coherent structures in the magnetopause: Recovery of static equilibria from single-spacecraft data. *J. Geophys. Res.* **104**, 6899. DOI. ADS.

He, W., Hu, Q., Jiang, C., Qiu, J., Prasad, A.: 2022, Quantitative Characterization of Magnetic Flux Rope Properties for Two Solar Eruption Events. *Astrophys. J.* **934**, 103. DOI. ADS.

Hu, Q.: 2017, The Grad-Shafranov Reconstruction in Twenty Years: 1996 - 2016. *Sci. China Earth Sciences* **60**, 1466. DOI. ADS.

Hu, Q.: 2021, Optimal Fitting of the Freidberg Solution to In Situ Spacecraft Measurements of Magnetic Clouds. *Sol. Phys.* **296**, 101. DOI. ADS.

Hu, Q.: 2023, Magnetic flux rope: What is it? *Journal of Physics: Conference Series* **2544**, 012002. DOI. https://doi.org/10.1088/1742-6596/2544/1/012002.

Hu, Q., Sonnerup, B.U.Ö.: 2001, Reconstruction of magnetic flux ropes in the solar wind. *Geophys. Res. Lett.* **28**, 467. DOI. ADS.

Hu, Q., Sonnerup, B.U.Ö.: 2002, Reconstruction of magnetic clouds in the solar wind: Orientations and configurations. *J. Geophys. Res.* **107**, 1142. DOI. ADS.

Hu, Q., He, W., Chen, Y.: 2022, A magnetic flux rope configuration derived by optimization of two-spacecraft In-situ measurements. *Frontiers in Physics* **10**, 960315. DOI. ADS.

Hu, Q., He, W., Zhao, L., Lu, E.: 2021, Configuration of a Magnetic Cloud from Solar Orbiter and Wind Spacecraft In-situ Measurements. *Frontiers in Physics* **9**, 407. DOI. ADS.

Hu, Q., He, W., Qiu, J., Vourlidas, A., Zhu, C.: 2021, On the Quasi-Three Dimensional Configuration of Magnetic Clouds. *Geophys. Res. Lett.* **48**, e2020GL090630. e2020GL090630 2020GL090630. DOI. https://agupubs.onlinelibrary.wiley.com/doi/abs/10.1029/2020GL090630.

Hu, Q., Zhu, C., He, W., Qiu, J., Jian, L.K., Prasad, A.: 2022, Validation and Interpretation of a Three-dimensional Configuration of a Magnetic Cloud Flux Rope. *Astrophys. J.* **934**, 50. DOI. ADS.

Kawano, H., Higuchi, T.: 1995, The bootstrap method in space physics: Error estimation for the minimum variance analysis. *Geophys. Res. Lett.* **22**, 307. DOI. https://agupubs.onlinelibrary.wiley.com/doi/abs/10.1029/94GL02969.

Lepping, R.P., Burlaga, L.F., Jones, J.A.: 1990, Magnetic field structure of interplanetary magnetic clouds at 1 AU. *J. Geophys. Res.* **95**, 11957. DOI. ADS.

Lepping, R.P., Burlaga, L.F., Szabo, A., Ogilvie, K.W., Mish, W.H., Vassiliadis, D., Lazarus, A.J., Steinberg, J.T., Farrugia, C.J., Janoo, L., Mariani, F.: 1997, The Wind magnetic cloud and events of October 18-20, 1995: Interplanetary properties and as triggers for geomagnetic activity. *J. Geophys. Res.* **102**, 14049. DOI. ADS.

Möstl, C., Davies, E.E., Weiler, E., Rüdisser, H.T., Amerstorfer, U.V., Weiss, A.J., Reiss, M.A., Majumdar, S., Horbury, T.S., Bale, S.D., Heyner, D.: 2026, On the Magnetic Field Evolution of Interplanetary Coronal Mass Ejections from 0.07 to 5.4 au. *Astrophys. J.* **1001**, 70. DOI. ADS.

Press, W.H., Teukolsky, S.A., Vetterling, W.T., Flannery, B.P.: 2007, *Numerical Recipes in C++ : The Art of Scientific Computing*, 778, Cambridge Univ. Press, New York. DOI. ADS.

Sonnerup, B.U.Ö., Guo, M.: 1996, Magnetopause transects. *Geophys. Res. Lett.* **23**, 3679. DOI. ADS.